Self-assembly synthesis and mechanism investigation of branched core–shell hybrids of tin nanowires and carbon nanotubes

Ruying Li,[a] Yong Zhang,[a] and Xueliang Sun[b]
Department of Mechanical and Materials Engineering, The University of Western Ontario, London, Ontario, Canada N6A 5B9

(Received 6 July 2012; accepted 26 October 2012)

Branched core–shell hybrids of tin nanowires and carbon nanotubes have been successfully obtained on silicon substrate via a self-assembly process by chemical vapor deposition. Structure characterization unveiled that the nanostructures are the hybrids of branched single-crystalline β-Sn nanowires coated with amorphous carbon nanotubes. Detailed investigation demonstrates that the amount of introduced ethylene plays a crucial role in triggering the morphology change of the product from freestanding core–shell hybrids to branched hybrids accompanying with a thickness and surface morphology change of carbon shell. Architecture of the branched core–shell hybrids has been categorized and the mechanism has been discussed. This kind of branched hybrids may find great potential applications in building multipath nanoelectronic components, lithium-ion battery electrodes, and enhanced superconducting nanodevices as well.

I. INTRODUCTION

Development of one-dimensional (1D) core–shell hybrid nanostructures has been a significant issue because of their great potential serving as building blocks in various nanodevices. Encapsulating nanowires inside carbon nanotubes may combine the functionality of both carbon nanotubes and target nanowires and possibly offer enhanced properties and more diverse applications of the nanowires due to the mutual coupling effect between the core and shell parts. Recently, various metal/alloy nanowires, including Pb and Bi,[1] Ni,[2,3] Ga,[4,5] Co,[6] Fe,[7,8] Pd,[9] Ag,[10] Cu,[11–13] CuSi,[14] FeCo,[15] and FeNi,[16] have been developed into core–shell structures coated with carbon nanotubes because of their applications in creating nanoscale thermometers,[4] switches,[5] rheostats,[11] magnets,[6,15,16] as well as electromagnetic shielding,[7] hydrogen storage,[9] and spot welding[12] nanodevices.

Bulk tin has superior electrical conductivity, resistance to corrosion, and high activity and has been extensively used in the electronic industry.[17–19] Superconducting behavior of tin nanowires has also been reported.[20,21] More recently, Zou and Wang[22] reported that tin@carbon core–shell nanowires have high and fast lithium storage capacities. On the other hand, excellent rate capability of branched tin-based alloy nanowires sheathing with carbon shell has been explored due to the increased electrolyte contact area and the reduced lithium diffusion length, which displays their promising potential in lithium-ion battery applications.[23] In addition, thickness of carbon layer plays an important role in cycle life of the lithium ion charge–discharge.[24]

In this paper, we report novel branched tin nanowire (single-crystalline)/carbon nanotube (amorphous) core–shell nanowires via a self-assembled chemical vapor deposition method on silicon wafer. The tin@carbon core–shell nanowires can be readily switched from freestanding structures to branched structures, and thickness of the carbon layer can be well controlled by tuning the amount of introduced carbon species. The branched core–shell nanowires reported here present a kind of architecture with multipaths, which can be an alternative structure unit for implementing multipath switching,[25] logic circuits,[26] lithium-ion batteries, and other complex functional nanoelectronic devices[27] as well as enhanced superconducting nanodevices.

II. EXPERIMENTAL SECTION

The multiterminal Sn@C core–shell nanowires were synthesized using a chemical vapor deposition method. In a typical procedure, pure commercial grade Sn powders (2 g, -325 mesh, 99.8%) were loaded in an alumina boat placed at the middle of a quartz tube horizontally mounted in a tube furnace. A piece of silicon wafer was placed beside Sn powder, acting as a substrate for collecting products. The reaction chamber was heated from room temperature to 900 °C at a heating rate of 50 °C/min under an atmosphere of flowing Ar (200 sccm) and controlled ethylene flow rate (0–9 sccm). Subsequently, the furnace was kept at 900 °C for 2 h and then was cooled to room temperature. After the reaction, gray dark-like products (thin films) were observed on the surface of the silicon wafer. In this work, no metal catalyst was predeposited on the silicon substrate.

[a]These authors contributed equally to this work
[b]Address all correspondence to this author.
e-mail: xsun@eng.uwo.ca
DOI: 10.1557/jmr.2012.381

Morphology of the synthesized product was examined initially using Hitachi S-2600N scanning electron microscope (SEM; Tokyo, Japan). Further structural characterization of the 1D nanostructures was carried out using a Rigaku-MiniFlex powder x-ray diffraction (XRD) spectrometer (Tokyo, Japan) and a JEOL 2010 FEG transmission electron microscope (TEM; JEOL Ltd., Tokyo, Japan) at 200 kV equipped with energy dispersive x-ray analysis facility. The crystal structure of the produced nanostructures was determined by high-resolution transmission electron microscope (HRTEM) and selected area electron diffraction (SAED) in a Tecnai G2 F30 TEM (FEI, Hillsboro, OR).

III. RESULTS AND DISCUSSION

Figure 1(a) shows a low magnification SEM image of the product; high-density nanowire arrays can be observed. A close-up SEM observation reveals that each nanowire bundle exhibits as a branched comb-like architecture with multiterminal nanowires, as shown in the typical picture of inset image. XRD was performed to investigate the phase structure of the product; the diffraction pattern shown in Fig. 1(b) can be indexed to β-Sn with tetragonal structure without graphite diffraction peaks being detected.

To shed a light on the detailed structure of the product, TEM experiment was conducted. Figure 2(a) shows a bright field image of the product; obviously, a branched core@shell core–shell nanowires structure is observed. It indicates that parallel distributed core–shell nanowires are connected at the cable end and a multiterminal core–shell nanowires are created, which is consistent with the results shown in the inset image of Fig. 1(a). As is known, the crystallinity nature of the nanocore and nanoshell as well as the core–shell interface determines the properties of the core–shell structure in practical applications. Therefore, scrutiny on the fine structure of the tin core, carbon shell, and the interface is necessary. HRTEM observation in Fig. 2(b) indicates the crystalline nature of the tin core; the spacing of the lattice fringes of the crystalline core is measured as 4.13 Å, corresponding to (110) planes of tetragonal β-Sn. The outer coat is mainly composed of amorphous carbon layer, while a couple of crystalline carbon layers are found at the core/shell interface due to relatively low catalytic effectiveness of tin. SAED pattern in Fig. 2(c) can be assigned to planes of single-crystalline tetragonal β-Sn. Therefore, the product is actually core–shell nanowires consisting of single-crystalline tin nanowires and amorphous carbon nanotubes, which is consistent with the XRD results.

To unveil the formation mechanism of the branched core–shell nanowires, effect of experimental conditions on the growth has been systematically investigated. During our experiments, it has been found that temperature and C_2H_4 dose are two important factors in determining the growth quality of the core–shell nanowires. When temperature was lower than 850 °C, the density of the core–shell nanowires was significantly decreased and branched core–shell nanowires could not be observed any more. While temperature decreased below 800 °C, 1D nanostructures were not observed any more based on SEM determination, which could be ascribed to low supersaturation degree of tin vapor. Branched core–shell nanowires were obtained at the temperature ranging from 850 to 950 °C, and 900 °C was fixed as the optimal temperature for the growth of branched core–shell nanowires. On the other hand, high temperature over 950 °C would terminate 1D growth of the nanostructures, and only microscale core–shell particles were observed, which was probably

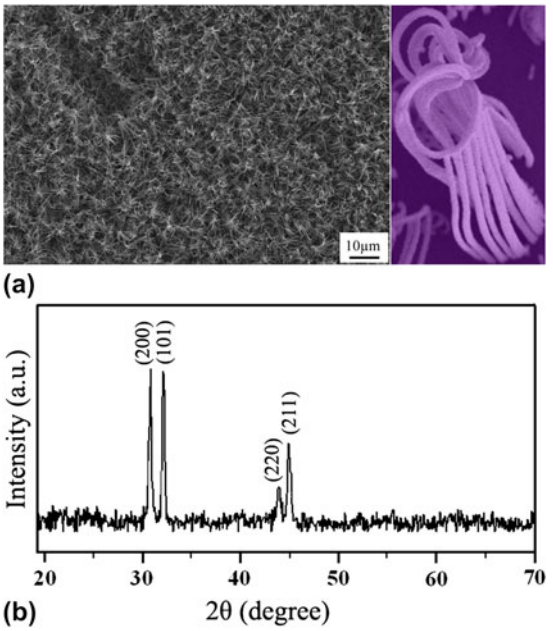

FIG. 1. (a) Typical SEM image, inset: magnified image; and (b) XRD pattern, of the branched core–shell nanowires.

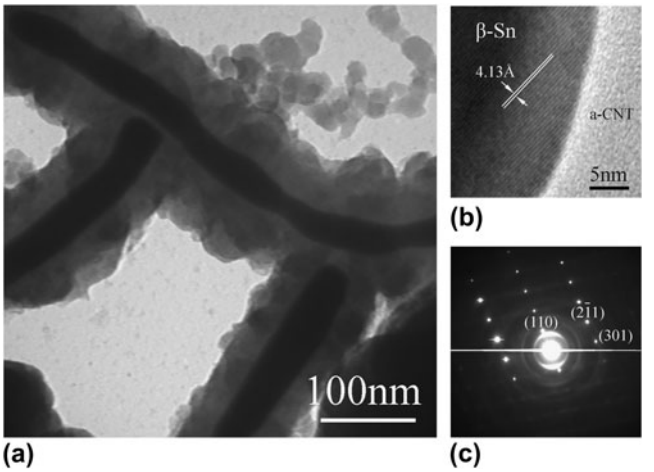

FIG. 2. (a) TEM image, (b) HRTEM image, and (c) SAED pattern of a typical branched core–shell nanowires.

due to high supersaturation degree of tin vapor leading to quick aggregation of liquid tin droplets during the deposition of tin vapor onto the silicon substrate. Moreover, experimental results showed that the amount of C_2H_4 gas plays a critical role in triggering the growth of the branched core–shell nanowires. Figure 3 shows SEM images of the product under different C_2H_4 flow rates. Without introducing C_2H_4, no 1D nanostructures but tin particles were observed on the silicon substrate. By introducing C_2H_4 with a flow rate of 1 sccm, freestanding 1D nanostructures were sparsely grown on the silicon substrate as shown in Fig. 3(a). Tuning the flow rate of C_2H_4 to 2 sccm, density of the 1D nanostructures was increased as shown in Fig. 3(b). When the flow rate of C_2H_4 was elevated to 5 sccm, branched 1D nanostructures were generated in bulk yield as shown in Fig. 3(c). Further increase of the C_2H_4 flow rate decreases the density of the branched core–shell nanowires. While the flow rate of C_2H_4 was increased to 9 sccm, 1D growth of the nanostructures was severely restrained and the branched 1D nanostructures also disappeared as shown in Fig. 3(d).

To shed light on the microstructure changes of the 1D nanostructures with C_2H_4 flow rate, Figs. 4(a)–4(c) show TEM images of the samples grown under a C_2H_4 flow rate of 1, 2, and 5 sccm, respectively. While the tin core tends to decline in diameter, the carbon shell exhibits significant increase in thickness with the C_2H_4 amount; the measured thickness of the carbon shell was around 10, 20, and 40 nm, respectively.

In terms of the growth of tin@carbon core–shell structure, it may follow the commonly used vapor–liquid–solid mechanism. At the target temperature, gaseous tin species generated from the molten tin powder were transported downstream on silicon substrate by argon gas and formed dispersed liquid tin droplets. The resultant tin liquid droplet provides an energetically favored site for the condensation of more incoming vapors, leading to the increase of the volume of liquid droplet. Liquid tin droplets, acting as catalysts, decomposed ethylene gas on the tin surface to form carbon nanotubes from the bottom of the tin droplet. As far as tin liquid core growth is concerned, the lateral growth of the liquid tin core is efficiently suppressed by the formation of carbon nanotubes at the side surface. In this case, the liquid tin is encapsulated inside tubular carbon. The coming tin species from vapor are absorbed on the top of the tin droplet to form 1D liquid tin core in the carbon nanotube. The continuous addition of C and Sn species at top surface of the nanostructure consequently leads to the 1D growth of tin/carbon core–shell nanowires structure. Figures 4(d)–4(f) show the surface morphology of the core–shell nanowires grown under the ethylene flow rate of 1, 5, and 7 sccm, respectively. It indicates that surface roughness of the carbon shell increases notably with the flow rate of ethylene.

However, another question may arise why branched core–shell nanowires were obtained at higher ethylene flow rate. Experimental results indicated that branched core–shell nanowires were seldom observed when the flow rate of C_2H_4 was low (below 5 sccm in this work). To disclose the relationship between the morphology and composition of the hybrid surface, electron energy loss spectroscopy (EELS) mapping technique was used. Figure 5 shows bright field image and EELS maps of a typical single Sn@C hybrid with

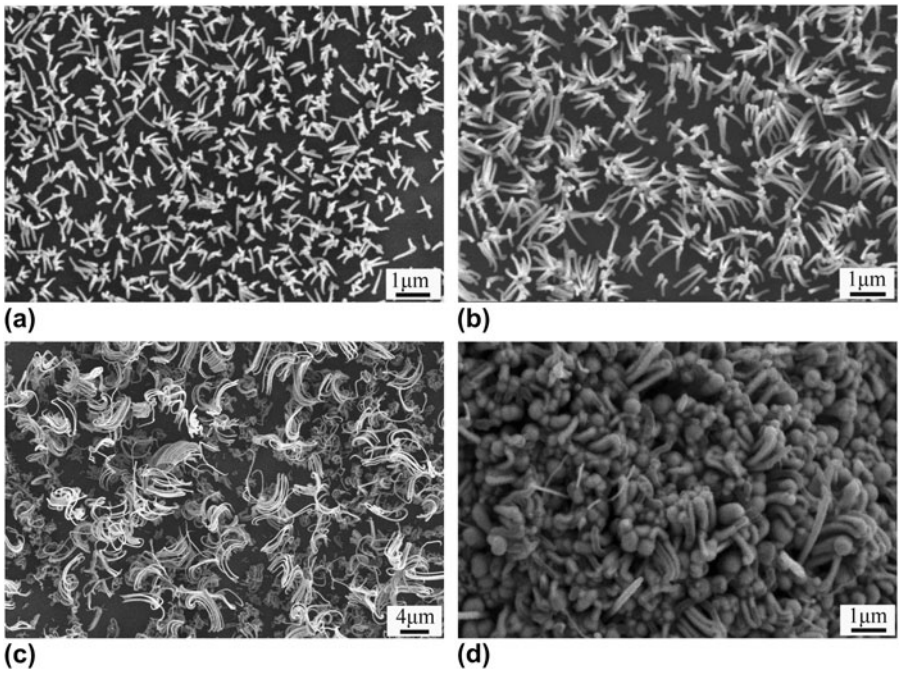

FIG. 3. SEM images of the product under the C_2H_4 flow rate of (a) 1 sccm, (b) 2 sccm, (c) 5 sccm, and (d) 9 sccm.

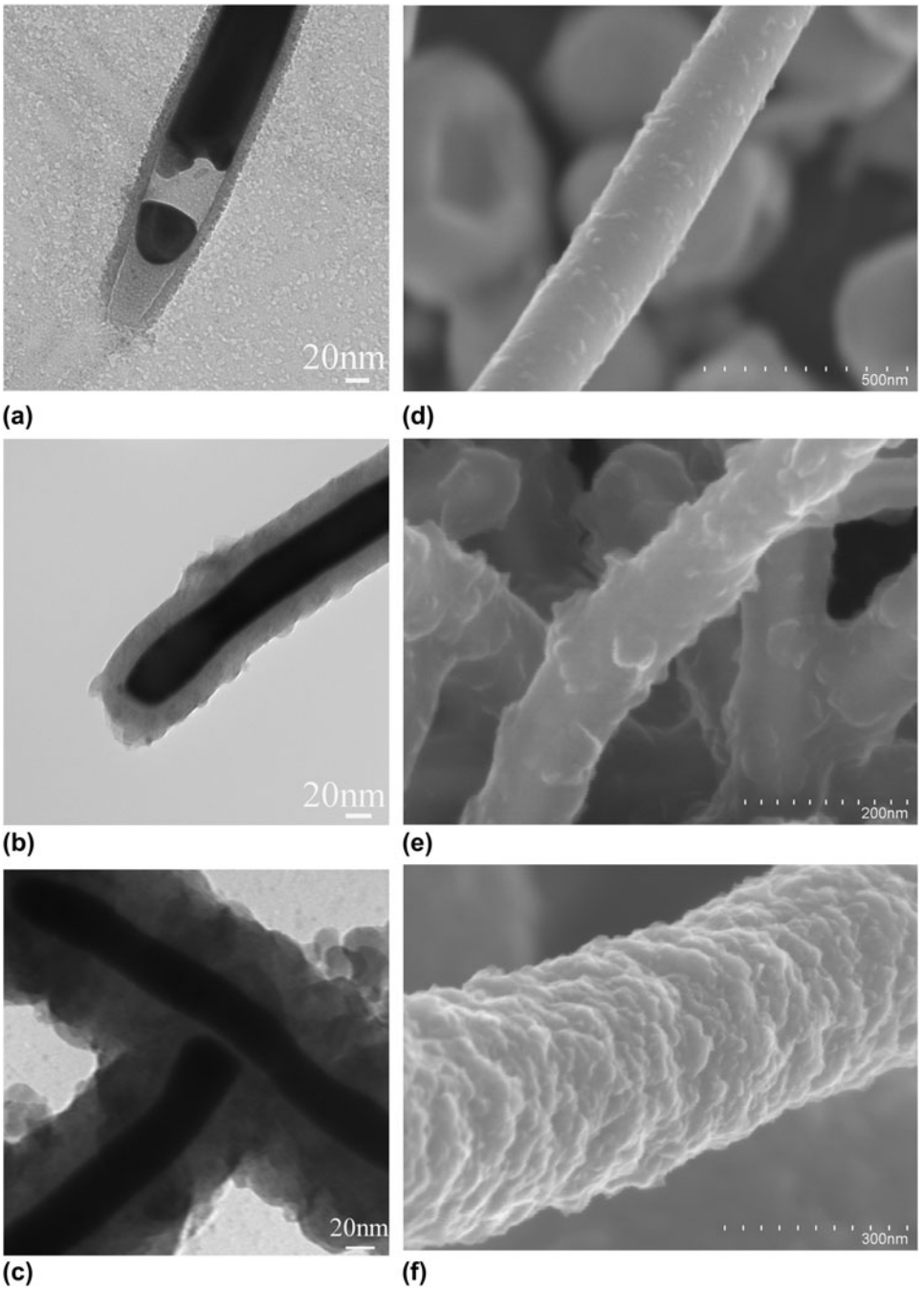

FIG. 4. TEM images of the Tin@C under the C_2H_4 flow rate of (a) 1 sccm, (b) 2 sccm, and (c) 5 sccm; SEM images of the Tin@C under the C_2H_4 flow rate of (d) 1 sccm, (e) 5 sccm, and (f) 7 sccm.

thin carbon layer. Figure 5(a) shows the bright field TEM image of the hybrid nanowires, while Figs. 5(b) and 5(c) display EELS mapping images of carbon and tin element in which bright region represents carbon and tin, respectively, in (b) and (c). Obviously, it shows that a tin nanowire is encapsulated inside a carbon nanotube. In addition, some small particles are found on the outer surface of the nanotube. Scrutiny of the EELS maps unveils that the particles are actually composed of both tin and carbon at the same place, which implies that deposition of tin and carbon occurred on the outer surface of the carbon nanotube during the growth and gave rough surface of the hybrid. A careful examination of the growth process has indicated that surface state of the carbon shell depends greatly on the concentration of ethylene, which is consistent with the results as shown in Fig. 4.

The growth of the core–shell nanowires involves the absorption and decomposition of ethylene, diffusion of carbon in the catalytic particle, and carbon precipitation

at its surface. When high concentration C_2H_4 was used, high supersaturation degree of carbon was formed in the tin liquid droplet, which resulted in larger thickness and roughness of the carbon shell, and the growth of branched hybrids was finally triggered with increasing ethylene amount.

According to previous literature,[28–31] it has been reported that interconnection architecture of branched nanostructures is crucial in determining physical and chemical properties of the branched nanostructures as well as their performance for various nanodevices. Therefore, it is an intriguing issue to

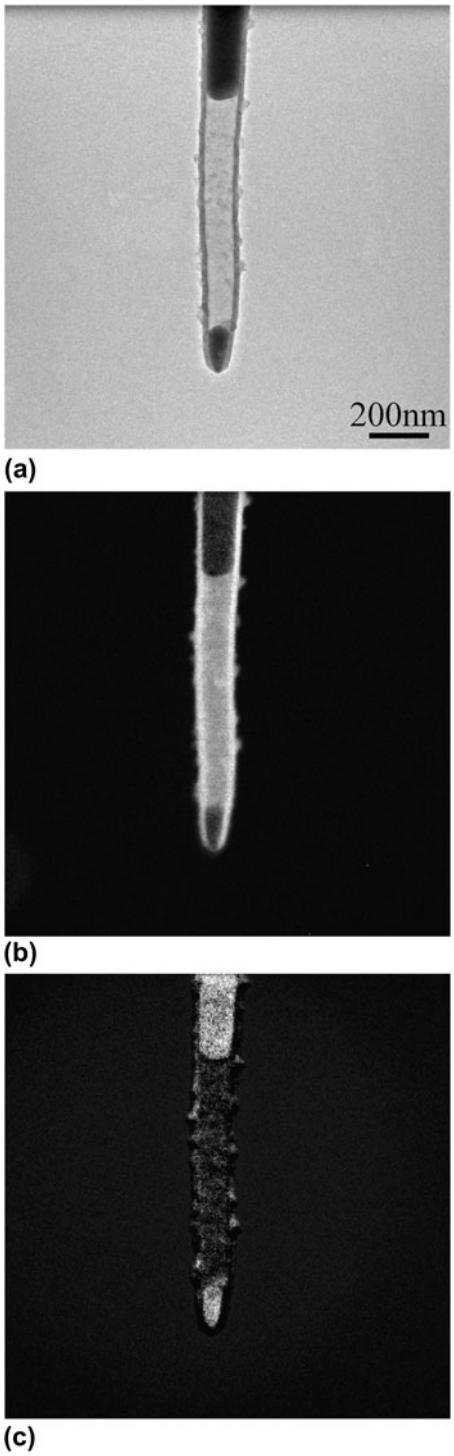

FIG. 5. (a) Bright field TEM image, EELS mapping images of (b) carbon and (c) tin element of the core–shell hybrid.

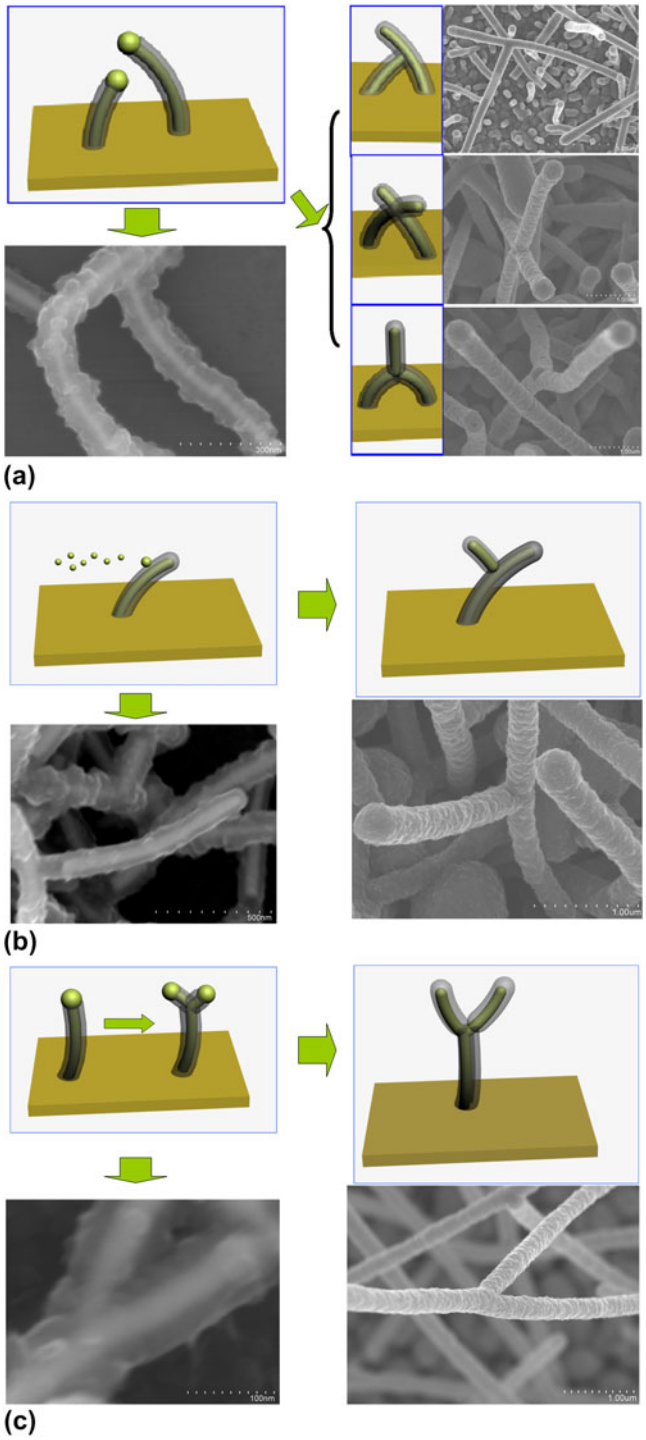

FIG. 6. Schematic diagram and SEM images illustrating the growth mechanism of the Tin@C core–shell nanowires with different morphologies (a) Type A, (b) Type B, and (c) Type C.

scrutinize the geometrical configuration of the branched tin@carbon core–shell nanowires. Through careful investigations on the growth process, branched core–shell nanowires with different geometrical configuration have been observed. Figure 6 illustrates the schematic growth diagram and corresponding SEM images of the branched structures. SEM images of the samples grown under the C_2H_4 flow rate of 5 and 7 sccm are shown here. Hereinto, the carbon shell of the sample grown under a C_2H_4 flow rate of 5 sccm is very thin so the core/shell contrast can be observed. Generally, the branched core–shell nanowires can be divided into three types, i.e., type A, B, and C as shown in Figs. 6(a)–6(c). Formation of type A branched structure can be described as the welding of two originally independent core–shell nanowires, and the three subtype branched core–shell nanowires are found in the product as shown in Fig. 5(a). For type B, as shown in Fig. 6(b), the outer surface of the first generation core–shell nanowires may collect the evaporated tin vapor and induce the nucleation and growth of the second generation core–shell nanowires. Different from type A branched core–shell nanowires, division of tin droplet core triggers the formation of type C branched core–shell nanowires as shown in Fig. 6(c).

Due to high surface roughness of the carbon shell, liquid end of other core–shell nanowires is attached to the carbon shell more readily, which triggered the formation of type A branched structure. In addition, rough surface of the carbon shell favors the collection of evaporated tin vapor, which would induce the nucleation and growth of type B branched core–shell nanowires. During the core–shell nanowire growth, division of the tin droplet might take place due to high precipitation rate of carbon clusters in the front end of the droplet, two carbon nanotubes could grow from the same catalyst simultaneously, and type C branched structures were generated. Compared with the most commonly used catalysts such as Fe, Co, Ni, and their alloys, the catalytic effectiveness of tin on carbon nanotube growth is lower because of the relatively low carbon solubility in tin, which may be one of the reasons why amorphous instead of graphite carbon shell was formed. Further research work is necessary to explore more detailed growth origin of the branched core–shell nanowires and achieve higher quality branched core–shell nanowires for practical applications.

IV. CONCLUSION

We have successfully prepared branched tin core/carbon shell core–shell nanowires on silicon substrate via a simple chemical vapor deposition method. The multiterminal feature of the core–shell nanowires is achieved as a result of self-assembled growth of aligned core–shell nanowires containing liquid tin core on silicon wafer. The tin core exhibits high quality single crystallinity, while the carbon shell shows amorphous nature. Low ethylene concentration favors the growth of freestanding core–shell nanowires, while high ethylene concentration triggers the achievement of branched core–shell nanowires. These high quality tin nanowires sheathed with protective carbon layer with multiterminals may find great potential applications in building multipath nanoelectronic devices, lithium-ion batteries, and enhanced superconducting nanodevices as well.

ACKNOWLEDGMENTS

This research was supported by Natural Sciences and Engineering Research Council of Canada, Canada Research Chair Program, Canada Foundation for Innovation, Ontario Early Researcher Award, and the University of Western Ontario. We thank Fred Pearson for fruitful discussion, structural characterization, and special support.

REFERENCES

1. P.M. Ajayan, T.W. Ebbesen, T. Ichihashi, S. Iijima, K. Tanigaki, and H. Hiura: Opening carbon nanotubes with oxygen and implications for filling. *Nature* **362**(6420), 522 (1993).
2. B.K. Pradhan, T. Kyotani, and A. Tomita: Nickel nanowires of 4 nm diameter in the cavity of carbon nanotubes. *Chem. Commun.* **14**, 1317 (1999).
3. Z.B. He, C.S. Lee, J.L. Maurice, D. Pribat, P. Haghi-Ashtiani, and C.S. Cojocaru: Vertically oriented nickel nanorod/carbon nanofiber core/shell structures synthesized by plasma-enhanced chemical vapor deposition. *Carbon* **49**(14), 4710 (2011).
4. Y.H. Gao and Y. Bando: Nanotechnology: Carbon nanothermometer containing gallium. *Nature* **415**, 599 (2002).
5. P.S. Dorozhkin, S.V. Tovstonog, D. Golberg, J.H. Zhan, Y. Ishikawa, M. Shiozawa, H. Nakanishi, K. Nakata, and Y. Bando: A Liquid-Ga-filled carbon nanotube: A miniaturized temperature sensor and electrical switch. *Small* **1**(11), 1088 (2005).
6. J.C. Bao, C.Y. Tie, Z. Xu, Z.Y. Suo, Q.F. Zhou, and J.M. Hong: A facile method for creating an array of metal-filled carbon nanotubes. *Adv.Mater.* **14**(20), 1483 (2002).
7. R.C. Che, L.M. Peng, X.F. Duan, Q. Chen, and X.L. Liang: Microwave absorption enhancement and complex permittivity and permeability of Fe encapsulated within carbon nanotubes. *Adv. Mater.* **16**(5), 401 (2004).
8. K. Svensson, H. Olin, and E. Olsson: Nanopipettes for metal transport. *Phys. Rev. Lett.* **93**(14), 1459011 (2004).
9. S. Toh, K. Kaneko, Y. Hayashi, T. Tokunaga, and W.J. Moon: Microstructure of metal-filled carbon nanotubes. *J. Electron Microsc.* **53**(2), 149 (2004).
10. D.K. Ma, M. Zhang, G.C. Xi, J.H. Zhang, and Y.T. Qian: Fabrication and characterization of ultralong Ag/C nanocables, carbonaceous nanotubes, and chainlike beta-Ag_2Se nanorods inside carbonaceous nanotubes. *Inorg. Chem.* **45**(12), 4845 (2006).
11. L.X. Dong, X.Y. Tao, L. Zhang, X.B. Zhang, and B.J. Nelson: Nanorobotic spot welding: Controlled metal deposition with attogram precision from copper-filled carbon nanotubes. *Nano Lett.*, **7**(1), 58 (2007).
12. D. Golberg, P.M.F.J. Costa, M. Mitome, S. Hampel, D. Haase, C. Mueller, A. Leonhardt, and Y. Bando: Copper-filled carbon nanotubes: Rheostatlike behavior and femtogram copper mass transport. *Adv. Mater.* **19**(15), 1937 (2007).

13. Y.X. Zhao, Y. Zhang, Y.P. Li, and Z.F. Yan: A flexible chemical vapor deposition method to synthesize copper@carbon core–shell structured nanowires and the study of their structural electrical properties. *New J. Chem.* **36**(5), 1161 (2012).
14. H. Guan, X. Wang, S.M. Chen, Y. Bando, and D. Golberg: Coaxial Cu-Si@C array electrodes for high-performance lithium ion batteries. *Chem. Commun.* **47**(44), 12098 (2011).
15. A.L. Elías, J.A. Rodríguez-Manzo, M.R. McCartney, D. Golberg, A. Zamudio, S.E. Baltazar, F. López-Urías, E. Muñoz-Sandoval, L. Gu, C.C. Tang, D.J. Smith, Y. Bando, H. Terrones, M. Terrones: Production and characterization of single-crystal FeCo nanowires inside carbon nanotubes. *Nano Lett.* **5**(3), 467 (2005).
16. R.T. Lv, A.Y. Cao, F.Y. Kang, W.X. Wang, J.Q. Wei, J.L. Gu, K.L. Wang, and D.H. Wu: Single-crystalline permalloy nanowires in carbon nanotubes: Enhanced encapsulation and magnetization. *J. Phys. Chem. C* **111**(30), 11475 (2007).
17. M.W. Barsoum, E.N. Hoffman, R.D. Doherty, S. Gupta, and A. Zavaliangos: Driving force and mechanism for spontaneous metal whisker formation. *Phys. Rev. Lett.* **93**(20), 206104 (2004).
18. Y. Chen, X. Cui, K. Zhang, D. Pan, S. Zhang, B. Wang, and J.G. Hou: Bulk-quantity synthesis and self-catalytic VLS growth of SnO_2 nanowires by lower-temperature evaporation. *Chem. Phys. Lett.* **369**(1–2), 16 (2003).
19. Z. Ying, Q. Wan, Z.T. Song, and S.L. Feng: SnO_2 nanowhiskers and their ethanol sensing characteristics. *Nanotechnology* **15**(11), 1682 (2004).
20. M.L. Tian, J.G. Wang, J. Snyder, J. Kurtz, Y. Liu, P. Schiffer, T.E. Mallouk, and M.H.W. Chan: Synthesis and characterization of superconducting single-crystal Sn nanowires. *Appl. Phys. Lett.* **83**, 1620 (2003).
21. Y.J. Hsu and S.Y. Lu: Vapor-solid growth of Sn nanowires: Growth mechanism and superconductivity. *J. Phys. Chem. B* **109**(10), 4398 (2005).
22. Y.Q. Zou and Y. Wang: Sn@CNT nanostructures Rooted in graphene with high and fast Li-storage capacities. *ACS Nano* **5** (10), 8108 (2011).
23. H. Lee and J. Cho: $Sn_{78}Ge_{22}$@carbon core-shell nanowires as fast and high-capacity lithium storage media. *Nano Lett.* **7**(9), 2638 (2007).
24. J. Cho: Control of the carbon shell thickness in $Sn_{70}Ge_{30}$@carbon core-shell nanoparticles using alkyl terminators: Its implication for high-capacity lithium battery anode materials. *Electrochim. Acta* **54**(2), 461 (2008).
25. S. Kasai, T. Nakamura, and Y. Shiratori: Multipath-switching device utilizing a GaAs-based multiterminal nanowire junction with size-controlled dual Schottky wrap gates. *Appl. Phys. Lett.* **90**, 2035041 (2007).
26. W.I. Park, J.S. Kim, G.C. Yi, and H.J. Lee: ZnO nanorod logic circuits. *Adv.Mater.* **17**(11), 1393–1397 (2005).
27. D.B. Suyatin, J. Sun, A. Fuhrer, D. Wallin, L.E. Fröberg, L.S. Karlsson, I. Maximov, L.R. Wallenberg, L. Samuelson, and H.Q. Xu: Electrical properties of self-assembled branched InAs nanowire junctions. *Nano Lett.* **8**(4), 1100 (2008).
28. X.H. Liu, Y.J. Lin, S. Zhou, S. Sheehan, and D.W. Wang: Complex nanostructures: Synthesis and energetic applications. *Energies* **3**, 285 (2010).
29. Q.Z. Cui, F. Gao, S. Mukherjee, and Z.Y. Gu: Joining and interconnect formation of nanowires and carbon nanotubes for nanoelectronics and nanosystems. *Small* **5**(11), 1246 (2009).
30. Y.W. Jun, J.S. Choi, and J.W. Cheon: Shape control of semiconductor and metal oxide nanocrystals through nonhydrolytic colloidal routes. *Angew. Chem. Int. Ed.* **45**, 3414 (2006).
31. K.A. Dick, K. Deppert, M.W. Larsson, T. Mårtensson, W. Seifert, L.R. Wallenberg, and L. Samuelson: Synthesis of branched 'nanotrees' by controlled seeding of multiple branching events. *Nat. Mater.* **3**, 380 (2004).